Civil, Architecture and Environmental Engineering

Editors: Jimmy C.M. Kao & Wen-Pei Sung

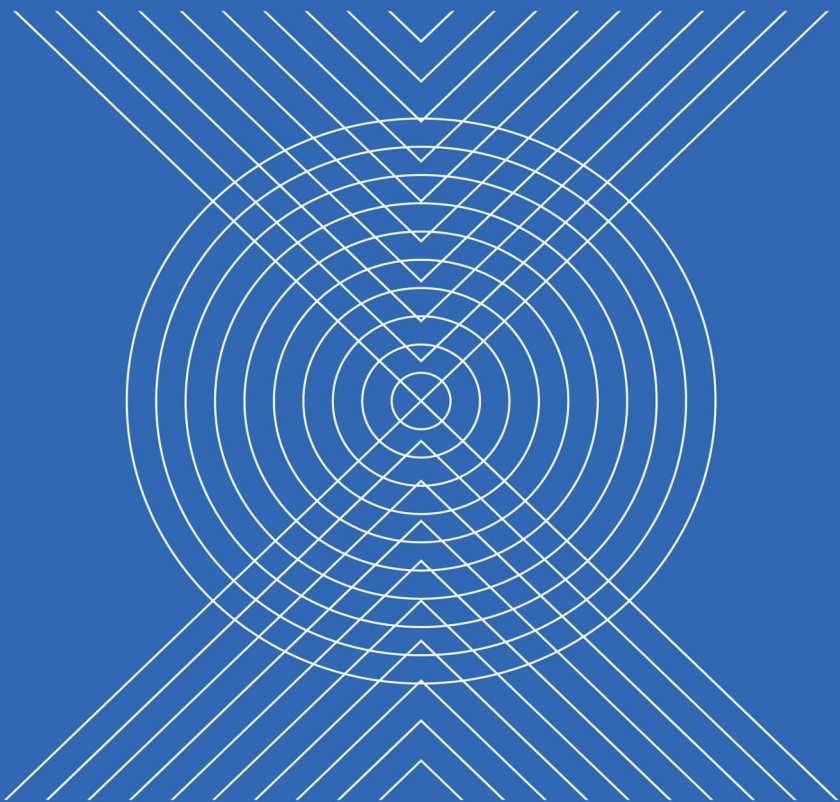

Two Volume set

CRC Press
Taylor & Francis Group
A BALKEMA BOOK

About the pagination of this eBook

This eBook contains a multi-volume set.

To navigate the front matter of this eBook by page number, you will need to use the volume number and the page number, separated by a hyphen.

For example, to go to page v of volume 1, type “1-v” in the Go box at the bottom of the screen and click "Go."

To go to page v of volume 2, type “2-v”… and so forth.

PROCEEDINGS OF THE INTERNATIONAL CONFERENCE ON CIVIL, ARCHITECTURE AND ENVIRONMENTAL ENGINEERING (ICCAE2016), TAIPEI, TAIWAN, 4–6 NOVEMBER 2016

Civil, Architecture and Environmental Engineering

Editors

Jimmy C.M. Kao
National Sun Yat-Sen University, Kaohsiung, Taiwan, R.O.C.

Wen-Pei Sung
National Chin-Yi University of Technology, Taiping City, Taiwan, R.O.C.

VOLUME 1

CRC Press
Taylor & Francis Group
Boca Raton London New York Leiden

CRC Press is an imprint of the
Taylor & Francis Group, an **informa** business

A BALKEMA BOOK

CRC Press/Balkema is an imprint of the Taylor & Francis Group, an informa business

Typeset by V Publishing Solutions Pvt Ltd., Chennai, India
Printed and bound in the UK and the US

Published by: CRC Press/Balkema
P.O. Box 11320, 2301 EH Leiden, The Netherlands
e-mail: Pub.NL@taylorandfrancis.com
www.crcpress.com – www.taylorandfrancis.com

ISBN: 978-1-138-02985-9 (set of 2 volumes)
ISBN: 978-1-138-06583-3 (Vol 1)
ISBN: 978-1-138-06584-0 (Vol 2)
ISBN: 978-1-315-22618-7 (eBook)

Civil, Architecture and Environmental Engineering – Kao & Sung (Eds)
© 2017 Taylor & Francis Group, ISBN 978-1-138-02985-9

Table of contents

Preface xxi

Organizing committee xxiii

Acknowledgements xxv

VOLUME 1

Structural science and architecture engineering

Visual support vector machine-based method for reliability-based design optimization 3
Y. Xie & Y.Z. Wu

Study on the tunnel group traffic accident risk using a fuzzy comprehensive evaluation model 9
B. Ma, R. Gao, Y. Gao, X.J. Wang & Z. Guo

Applications of new reinforcement methods in city tunnels for shield launching and arriving 13
H. Jun, J.B. Shi, W. Hong & W. Xiaobin

Research on the stress characteristics of concrete carrier pile based on finite element analysis 19
J.Y. Li, A.Q. Zhang & X.G. Han

Theoretical analysis of the deformation of shield tunnel segment under fire 25
X.B. Han, Y.X. Xia & L.L. Chai

Optimization of composition of the claddings of wooden structures 31
M. Halirova, H. Sevcikova, R. Fabian, E. Machovcakova & R. Janousek

Evaluation of the ultimate strength of RC I-shaped members subjected to a combined action 37
P. Wang, Z. Huang & Q.S. Wang

Three-dimensional centrifuge and numerical modeling of pile group due to twin tunnelling in different depth 43
S.K. Ma, Y. Shao, Y. Liu, J.Y. Chen & J. Jiang

Index selection and weight analysis of the underground development of urban municipal public facilities 49
L. Ye & L.M. Zhu

Risk assessment of pipelines in operation based on AHP and application of MATLAB 55
L. Chen, G.X. Wang & J. Zhao

Effect of ground co006Editions on design parameters for bridge foundations 61
M.T.A. Chaudhary

Research on multisource information fusion of tunnel geological prediction based on evidence theory 67
Z.H. Liu, Y.T. Wang, H. Ke, H. Wu & D. Zhou

Pushover analysis of modularized prefabricated column-tree steel frame 75
Z.P. Guo, A.L. Zhang & X.C. Liu

Study on reuse of heritages of an old industrial area in Harbin Gongyijie area against the backdrop of urban renewal 83
X.Z. Shan & W. Cheng

Research on lateral resistant behavior and design of multicover plates connection for prefabricated steel plate shear wall with beam-only-connected infill plate 89
X. Zhang, A.L. Zhang & X.C. Liu

Research on sensitivity and control criteria of cable length error in a double-strut cable dome 97
C. Sun & A.L. Zhang

Structural design of a prefabricated steel frame structure with inclined braces 105
X.C. Liu, H.X. Wang & Z.P. Guo

A study on the design of an ungated community 115
F. Jia, R.X. Wang & F.L. Ma

Protection and utilization of Gaichun Garden ruins of the Summer Palace 119
D. Zhao & L. Zhang

Development of a web-based hybrid BIM cost-estimating system for fire safety engineering 125
M.-H. Wen, W.-C. Huang & Y.-W. Wu

Test and parametric analysis of postfire seismic performance of SRC column–RC beam joints 135
G.H. Li, L. Xie & D.F. Zhao

Using agent-based simulation approach for estimating the efficiency of the building project design team 139
M.H. Tsai

Field assessment of window daylighting with prismatic glazing 145
Z. Tian, D. Xue & Y.P. Lei

Mechanical analysis of rockburst considering the "locked in" stress in the driving face of the roadway 149
X.-B. Yang, X.-X. Han, H. Wang & T.-B. Zhou

Study on the identification of major safety defects in port engineering 155
J.H. Peng

Investigating the impact of greenery on the driver's psychology at a freeway tunnel portal 159
D.Q. Xiao, Z.W. Shen & X.C. Xu

Modeling two-dimensional rubble mound breakwater using dolos at armor layer and geotube at the core layer 167
O.C. Pattipawaej & H.J. Dani

Shear stress calculation of rubber asphalt overlay and stress-absorbing layer 171
J.Z. Tan, J.G. Wei, C. Pan & K.X. Huang

Experimental study on beam-column joints of new prefabricate assembly frame structures 177
W.Z. Zhu & J.C. Zhang

Seismic analysis of large span spatial steel frame with isolation system 185
W.Z. Zhu

Effect of material ingredients on the cement-based self-leveling material 195
J. Liu, J.J. Hu, R.Q. Liu & Y.Q. Yang

Rebuilding the city parks: How great is the effectiveness of environment-friendly constructions? 201
R.Y. Tallar, A.F. Setiawan & J.P. Suen

Renaissance with recycled materials: Reconstruction of Guifeng Temple 205
Y.S. Gao & J. Xu

Research on safety management of construction projects based on game theory 209
J.X. Zhao, M.M. Wang, J.H. Sun & K. Li

Prestress distribution calculation method of a ridge tube cable dome with annular struts 215
A.L. Zhang, Y. Bai, X.C. Liu & C. Sun

A new multiple-model analysis method considering structural uncertainty 223
F.Q. Zhu

Promotion of transportation on urban spatial distribution and industrial development in Beijing 227
X. Peng

Selection of interruptive protection methods in rapid transit underground construction 233
H.-C. Yang & C.-C. Liu

Damage mechanism and dynamic analysis of tunnel lining structures under internal blast loading 239
C.Y. Chen, Y.B. Jiang, J. Yang, L.F. Zheng & Z.P. Li

The seismic responses of near-fault frame structure cluster on basin induced by the rupture of reverse fault 247
W. Zhong

Wave propagation FEA and experimental validation of aluminum plate using piezoelectric elements 253
S. Yan, S. Zhang, Z.Q. Wang, P.T. Zhao & Y. Dai

Numerical simulation on seismic behavior of subway station structure under near-fault ground motions 259
B.Z. Tang, S. Chen, X.J. Li & H.Y. Zhuang

Finite—infinite element analysis of soil dynamic response under moving load 265
C.Q. Tian & L.Q. Yuan

Evaluation of the processing suitability of rural domestic sewage treatment, taking Fangshan in Beijing as a case study 269
Y. Wang

Influence analysis of the incremental launching of steel box girder and local stability control 275
F.-J. Xie

Study on active strategies for thermal environment regulation in the zero-energy houses of Solar Decathlon, China 285
F. Shi, W. Jin, W.W. Zheng & T. Zhuang

Research and enlightening of ecological infrastructure-oriented "multiple planning integration" based on Germany's spatial order and structure planning—illustrated by the example of Dujiangyan 289
Y.J. Li, F. Fu & Y. Yi

Homogeneous generalized yield function and limit analysis of structures with rectangular sections 295
W. Ou, L.F. Yang & W. Zhang

Numerical simulation analysis of the influence of shield tunneling on an adjacent tunnel 301
M.D. He & J. Liu

Development and validation of the effective stress algorithm of the Davidenkov constitutive model using the Byrne pore pressure increment model 309
B. Ruan, G.X. Chen & D.F. Zhao

Urban ITS framework and essential parts of the ITS frame structure 317
M.-Q. Li, Z.-H. Wang, W. Wan & Z.-T. Jing

Development and implementation of a product module division system based on the function–principle–structure 321
J. Chen, L.M. Wang & L.L. Yang

Parameter optimization of space truss and aerospace load viscoelastic damping composite structure 325
Z.W. Zhang, P. Wang & H.T. Luo

A unified theory of thermodynamically consistent microplane elastoplastic damage, and elastoplastic damage models 331
W.S. Li & J.Y. Wu

Building materials and materials science

Preparation of sebacic acid by a phenol-free method 341
L. Xu, L.L. Mao, Y.M. Feng, J.C. Zhang, M. Wang, T.T. Zhao, X.J. Gao & R. Ren

Effects of electrospinning parameters on the pore structure of porous nanofibers 345
Z.Y. Sun & L. Xu

Preparation of orderly nanofibers using bubble-electrospinning 349
Z.B. Shao & L. Xu

Environmental radioactivity measure and dose estimation of ^{90}Sr in some area 353
L. Ma, X. Ren & K. Zhang

Effect of humic acid on the adsorption of levofloxacin to goethite 357
X.P. Qin, H. Hou, L. Zhao, J. Ma, Z.J. Sun, W.J. Xue, F. Liu & G.C. Wang

Calcium and manganese affect ethanol fermentation by *Pichia stipitis* in cadmium-containing medium by inhibiting cadmium uptake 363
M.-T. Gao, X.X. Chen, W. Zheng, Q.Y. Xu & J.J. Hu

Performance comparison of Biological Aerated Filters packed with plolyurethane sponge and ceramic particles 367
G.L. Yu, X.J. Yan, H. Chen, C.Y. Du, Y.J. Fu & J.X. Zhang

Preparation and evaluation of the Ni-Al catalyst derived from LDHs synthesized on γ-Al_2O_3 support 373
X.K. Zhao, Y.Q. Li, Y. Xu, X.H. Du & J.J. Xu

Synthesis and hydrodesulfurization performance of NiMo sulfide catalysts supported on an Al-Si mixed oxide 377
Q. Yu, J.C. Zhang, J. Nan, H.B. Yu, X.F. Peng, H. Xiao, G.L. Song, S.Q. Zhang, S. Wang, Y.T. Zhang & G.H. Zhang

Study on solidification of Ningbo mucky soil 381
J.Y. Lu, R.Q. Xu, Q. Yan & X. Wang

A study on the utilization of iron and steel industrial solid waste 387
Y.B. Zhang, R. Zhu, Y. Wang, C.S. Yue & X.J. Piao

Experimental study of the drainage and consolidation characteristics of tailings discharge and accumulation by gradual height rising under the action of drainage material 393
J. Su, X.D. Ou & K.W. Hou

LQR control of across-wind responses of tall buildings using composite tuned mass dampers 403
Y.M. Kim, K.P. You, J.Y. You, S.Y. Paek & B.H. Nam

Time-dependent reliability analysis of steel fiber-reinforced concrete beams under sustained loads 411
Y. Li, K.H. Tan & S.-M. Yu

Research on the heat transfer characteristics of rock and soil under the effects of vertical double U-type buried-pipe heat exchanger 417
X.-D. Ou, X. Pan, H. Dai, Y.-C. Tang & Z.-Y. Liu

Nitrogen removal performance of ANAMMOX-PVA granules immobilized by different preparation methods 425
Y.M. Han

Seismic response of a long-span cable-stayed bridge with slip-shear metal damper 429
C.K. Jiao & X. Dong

Research on the interfacial bond behavior between CFRP sheet and steel plate under the static load 435
L. Zhang & S.-Y. Cao

Influence of thick and loose sediments on the vacuum load transfer 439
J.X. Weng

Enhancement on fireproof performance of construction coatings using calcium sulfate whiskers prepared from wastewater 447
T.-P. Tsai & H.-C. Yang

Simulation of nonlinear ultrasonic waves in anisotropic materials using convolution quadrature time-domain boundary element method 451
T. Saitoh, T. Maruyama & A. Furukawa

Study on the layout method of newly-added feeder bus lines coordinating with bus rapid transit 457
Z. Guo, P.H. Wei, X. Peng, C.Z. Chang, L. Tong & J.M. Velásquez

Design of a campus view of a virtual roaming system based on VR 465
L. Yu

Analysis on sustainable financial framework and fare adjustment strategy of China's urban public transit 471
S. Xu, C. Li, X.L. Liu & Y.K. Du

Sanitation improvement and the bottleneck analysis of equity in China: From the perspective of specialists 479
X.L. Li & Y.Q. Miao

Ultimate capacity of uniaxially compressed perforated steel plates strengthened by using CFRPs 483
X. Tao & S.Y. Cao

Research on the measurement of the permeability coefficient of porous asphalt pavement 489
G.Q. Tang, L. Gao, T.J. Ji & J.G. Xie

Mechanical performances of icing atop cement concrete surfaces coated with emulsion wax curing agents 495
J.-L. Yao & M.-J. Qu

A study on residential area's adaptability design for the aged in China based on open building theory 501
X. Meng & B.C. Fu

Safety management strategies for public infrastructure projects 507
C.W. Liao & T.L. Chiang

The influence of the horizontal load on the stress–strain relationship of an asphalt layer 511
Y.H. Wang, X.M. Tan, X.J. He, Y. Wang, C. Wang & T. Liu

A study on the protection type of flow-guided porthole dies with twin cavities for semi-hollow Al-profiles 517
R.R. Deng & P. Yun

A study on covering and protection type porthole dies for semi-hollow Al-profiles 521
R.R. Deng & P. Yun

A study on protection type porthole dies of semi-hollow Al-profiles with four cavities 525
R.R. Deng & P. Yun

Numerical and experimental study on stability of aluminium alloy riveted and stiffened panels under in-plane shear 531
D.W. Wang, Z.K. Lei, R.X. Bai & Y. Ma

Process optimization for the new nano-complex internal coating and its anti-corrosion and drag reduction properties in natural gas pipes 535
B.H. Hao, B. Sun, Z.H. Liu, Y.L. Han & L.F. Zhao

An improved gray wolf optimization algorithm and its application in iron removal from zinc sulfate solution using goethite 539
T.B. Wu, J.H. Liu, Y.L. Liu, Q.M. Zhao & X.J. Li

Determination of multi-element in abstergent by ICP-MS with microwave digestion 545
B.L. Wu, Z.X. Wang, J.M. Ye, Z.X. Lin, H. Wang & C. Luo

Fabrication and application of superhydrophobic-superoleophilic porous Cu sponge 549
Y.J. Xing, Z.J. Han, J.L. Song, J. Sun, J. Luo, Z.A. Liu, J.Y. Liu, L. Huang & X. Liu

Preparation of porous ceramics using $CaCO_3$ as the foaming agent 555
J. Li & Y.L. Chen

Spacing optimization modeling and simulation of thermo-optic VOA gold thin film interconnect 559
S.T. Ding, L. Xu, F. Huang & M.L. Gong

Growth and characterization of thick Ge epilayers on Si and Silicon-on-Insulator (SOI) substrates with low temperature Ge buffers 565
Z.W. Zhou

Effect of $ZnSO_4$ and $SnSO_4$ additions on the morphological of α-Al_2O_3 flakes for pearlescent pigment 569
H. Qin, L. Wang & Y. Xiong

A facile cost-effective method for preparing superhydrophobic carbon black coating on Al substrate 573
P. Wang, B. Sun, T. Yao, X. Fan, C. Wang, C. Niu, H. Han & Y. Shi

Preparation of multifunctional flake alumina ceramics 577
Q.R. Wang, C. Liu, K.X. Du & Y. Xiong

Study on the deformation of plastic films by virtual particle method 581
X.H. Yang, Z. Yang, Y.X. Wang, C.Y. Lv & X. Cheng

An experimental study of installing-holes distances parameter optimization for metallic inserts bonded into CFRP laminates 585
J. Liu, H. Zhang & K. Hou

Formation and test methods of the thermo-residual stresses for thermoplastic polymer matrix composites 589
C.C. Wang, G.Q. Yue, J.Z. Zhang, J.G. Liu & J. Li

Effects of lithium slag from lepidolite on Portland cement concrete 593
Q. Luo, Y.F. Wen, S.W. Huang, W.L. Peng, J.Y. Li & Y.X. Zhou

Sorption properties of TEMPO-oxidized natural cellulose to iron ions 597
C.Z. Geng, Y.H. Lou, D.Y. Yan, Z.H. Zhao, Z.X. Xue & Y.Z. Xia

Research on the precision of grinding experiments in an iron ore 603
G.M. Shi, L.P. Jiang, J.M. Zhao, R.Q. Zhao, Y.C. Zhou & S.C. He

Construction equipment and mechanical science

An experimental study on the dynamic characteristics of compact transmission lines bundles following ice shedding 609
K.P. Ji, B. Liu, X.P. Zhan, X.Z. Fei, C. Deng & L. Liu

A single-lens optimal imaging system based on a liquid crystal spatial light modulator and micro-scanning optical wedge 613
N. Xu, Z.-Y. Liu & D. Pu

A geometry-based path optimization approach for motion control of the NC grinding machine 621
F. Zhang, J. Gong, Y.J. Liu, W. Xia, M.F. Huang & Y.F. Fu

A study on carbon electrode-based photoelectrochemical-type self-powered high-performance UV detectors 625
Q. Meng, X. Fan, E.Q. Wu & L. Chu

A scheme study of CFB power generation by using pet coke 629
H.T. Liu, L. Xue & D.F. Xu

Design of the pilot-scale double effect evaporator for high-concentration sodium hydroxide production 633
L. Gao

Early fault diagnosis of wind turbine gearboxes based on the DSmT 641
Z.Q. Liu & G.C. Chen

A study of an improved method for horizontal alignment based on the line element 647
Y.H. Li, Y.J. Liu & Y.L. Li

Theoretical analysis of mechanical properties and mechanical design for fabricated zero initial cable force friction dissipation 651
Q.X. Ye & A.L. Zhang

An optimal allocation model of residual control rights in the hydraulic PPP project 659
Y.H. Zhang, J.C. Feng, S. Xue & K. Zhang

A study on the optimized hydraulic circulation system of the artificial lake 665
Q.N. Jin, A.J. You & H.B. Xu

Development of new elastic constant estimation method using laser ultrasonic visualization testing 669
T. Saitoh & A. Mori

Selection for the frequency control point of the VAV air supply system in large underground spaces 675
K.D. Xue, Z.H. Zhou, Y.F. Zhang & Y.M. Sun

The innovations of the ship lock design for the Tugutang Hydropower Station in the Xiangjiang river 679
H.Y. Liu & C.Y. Wang

Knowledge management in construction—the framework of high value density knowledge discovery with graph database 685
Y. Jing, Y.-C. Wang & Z. Wang

Research of cold region green hospital design specification and practice 689
Y.Z. Gao, H.Y. Mei & J.F. Dong

Development of intelligent residual current devices based on the PIC micro-controller 693
H. Chen, J. Xiang, R. Huang, L.M. Shen, F.S. Chen, K. Li, W.N. Wang, L.M. Bu, X. He & X.Y. Xu

Design of Control Moment Gyro equivalent sound source based on transfer function matrix inversion 699
W. Cheng, W.-Q. Sun, G.-Y. Wang, J.-P. Chen, X.-F. Li & J. Jia

A study of the magnetic field distribution with saddle-shaped coil of the electromagnetic flow meter 707
H. Jia, Y.M. Wang, W.T. Li & Y.Y. Zhang

A study on a localizable CMOS temperature sensor based on wireless transmission 713
L.Y. Chen, J.Q. Li & Y.X. Li

Finite element analysis of the roller coaster wheel bridge based on virtual prototype technology 719
Y.M. Wang, J. Ye, X.T. Xu & S. Song

Multi-axis coordination control based on siemens S7-CPU315T 725
C.H. Pan, Y.L. Li & M.W. Qin

Short-term photovoltaic power forecasting based on the human body amenity and least squares support vector machine with fruit fly optimization algorithm 729
H.B. Chen, W. Han & L. Chen

An RFID-enabled CEP model for cloud manufacturing shopfloor 735
K.Q. Chen, Y.Y. Qiu, M.L. Wang, Q.Y. Dai, R.Y. Zhong & C.M. Huang

Optimization of extraction of polysaccharides from mulberries by using high-intensity Pulsed Electric Fields 741
S.L. Jin

Stress analysis of the interference fit in helical gear transmission 747
T. Zhao

A review of transformerless DC–DC boost converters for renewable energy sources 753
J. Luo

The linear fatigue cumulative damage analysis of the welding seam 759
Y.Y. Wang

Application of wavelet analysis and resonance demodulation in mechanical fault diagnosis 765
C.H. Shen & W. Wang

A study on the modeling of the slider-crank mechanism based on parameter identification 769
X.J. Wang, X.H. Tang & J. Shen

Angle measurement by comparing the amplitude technique of the sum-difference pattern radiometer 775
H. Wang, J. Xiao & B. Bi

Tension control methodology of active continuous discharge and intermittent reciprocating work based on master-slave synchronous motion 781
L. Han, H. Hu, W.H. Ding & J.Y. Li

Design and kinematics analysis of a novel liquid-brewing steamer feeding robot 787
J.S. Zhang, B. Li, T.C. Zhang & X.H. Zhao

Design and simulation analysis of a new type of multi-gear pump 793
X.H. Zhang, P.Y. Liu, W.J. Wei, H.T. Li & G.P. Tian

A study on the torsional fatigue fracture location of steel wires 799
W.J. Wei, D.C. Wang, P. Cheng & C.X. Shao

The lightweight design of the support arm 805
Y.Q. Tian, D. Meng & X.Y. Lin

An analysis of the thermal elastohydrodynamic lubrication performance of the slope of the thrust bearing 809
Y.L. Liu, Y.H. Li, T.Y. Niu, J.F. Huang & Y.X. Wang

Simulation of submarine underwater motion with an external weapon module 815
Y.Q. Lian, C.L. Li & Y. Liu

A multi-objective NC drilling parameter optimization model to achieve low energy consumption and costs 823
W. Yan, H. Zhang & Z.G. Jiang

An experimental study of the dynamic equivalence leakage of rolling-piston compressors 827
K.H. Geng, W. Wei, X.B. Ma, X. Wang, X.G. Han, T.B. Zhao, C.L. Chen & H. Sun

The structure and transmission efficiency analysis research of a new pattern F2C-T pin–cycloid planetary transmission 833
L. Xuan, H. Jiang & T.M. Guan

A study on surface zinc plating and heat treatment of welding gears 839
R. Zeng, J.H. Luo, Z.R. Lin & L.L. Wang

Development and application of a test platform for a battery management system 843
J. Xiong, Z.H. Jin & Z.C. Li

Experimental study on yarn friction slip in the yarn pull-out test 847
W.K. Li, Z.K. Lei, F.Y. Qin, R.X. Ba & Q.C. Fang

Analysis and research into the effect of dithering technology on ADC's SNR 851
K.K. Jin & X.L. Chen

Design and implementation of a CANopen master stack for servomotor controllers in a 6-DoF manipulator 855
J.H. Ji, Z.H. Tao, T. Zhang & M.Z. Qi

Design of a crane intelligent control system 861
C.C. Zhang, S.G. Liu & H.W. Xie

Valve clearance fault diagnosis of an internal combustion engine based on wavelet packets and k-nearest neighbors 865
R. Tan, Y. Zhang, T.X. Zheng, B. Yang & Y.J. Wang

RV reducer dynamic and static performance test system design 871
W.-B. Fu, C.-S. Ai, C.-L. Tang, Y.-S. Yang, G.-P. Li & H.-H. Zhao

Analysis of automotive suspension compliance based on the main effects of rubber bushing 877
B. Chen, J.-H. Fu & Z.-M. Chen

Experimental and simulation research on the friction and wear properties of surface textured friction pairs in CST 883
S.N. Sun, L.Y. Xie & R.S. Long

Simulation and analysis of MPPT used in photovoltaic grid-connected systems based on the improved disturb-and-observe method 889
J.F. Wang & H.R. Zhao

Automatic control loop optimization method of thermal power plant based on internal model control 895
S. Gao, X.K. Pang, J. Li, C.W. Li & H.D. Li

Multidisciplinary optimization and parameter analysis of the in-wheel permanent magnet synchronous motor of a tram 899
X.C. Wang & Z.G. Lu

Dynamic simulation and muzzle vibration analysis of vehicle-mounted automatic mortar 907
Y. Fang, J.-Q. Qin & C.-C. Di

Numerical simulation of aspheric glass lens during the non-isothermal molding process 911
H.J. Duan, Z.L. Xiao & J.Y. Tao

Temperature field analysis of a porous modified concrete composite pavement 915
Y.H. Wang, X.M. Tan, X.J. He, T. Liu, Y. Wang & C. Wang

A retrieval method based on a CBR finite element template 921
Q.Y. Ma, D.P. Xie, L.H. Song & M.J. Zhou

Improved reduction of graphene oxide through femtosecond laser pulse trains 927
R.Y. Yan, P. Zuo & X.J. Li

A nanoparticle-decorated silicon substrate for SERS via circularly polarized laser one-step irradiation 931
G. Meng, P. Ran & Y.D. Xu

An experimental study on rotation ultrasound-assisted drilling for high-strength engineering of mechanical connection components 935
S. Hong

Synthesis of PbO nanosheet-based thin films for all-solid-state supercapacitors 939
J. Zhang, H.Y. Xie & Z.J. Chen

A large-scale SERS substrate fabricated by using femtosecond laser with superhydrophobicity 945
Y.D. Xu, G. Meng & P. Ran

A study on the ship model resistance test and numerical simulation 949
H.C. Pan, S.N. Yu & Y.J. Yang

Magnetic memory testing signal analysis of Q345 steel welding parts under the static tension condition 955
M. Lou, X.-H. Lv, F. Lu & B. Li

Research on reliability assessment of success or failure product based on small sample 959
H.-P. Li, Z.-L. Xuan & Y.-D. Wang

Numerical simulation of hydroforming of a stainless steel sink 965
Q.H. Li, P. Zhu, X.Q. Guo, J.W. Hou & X.M. Li

The fabrication and measurement of a bi-axial thermal convection acceleration sensor 971
H. Wang, Y.G. Li, P. Yan, Y. Huang & S. Sugiyama

Innovative green design of the frog ramming machine based on TRIZ/FRT 975
Z.G. Xu, J.L. Li & Z.Y. Zhu

Rotor fault diagnosis based on SVM and improved D–S theory 979
Z.-H. Yan & P. Liao

A study of the relationship between pre-tightening force and torque in precision instrument assembly 985
S. Huang, X. Jin, Z.F. Wang, Z.J. Zhang, M.Z. Xiao & C. Cui

Thermal characteristic analysis of a hollow screw based on the fluid structure thermal coupling 991
X.S. Li, W. Xiong & J.N. Xu

Research on intelligent exhaust device design of the breaker in the substation 995
X. Yu & W. Wang

An improved calibration method for a nondestructive testing system based on infrared thermopile sensors 999
W. He, T. Zhou, B. Jiang, Y. Wan & Y. Su

Evaluation of wind turbine power generation performance based on a multiple distribution model 1005
S.Q. Guo, J.R. Yang & H. Li

Research on the acoustic emission testing of the tank truck and on the defect acoustic emission source location method 1011
Z.W. Ling, M.L. Zheng, D. Bin & X.L. Guo

Nonlinear dynamic analysis of a cantilever plate for generating electricity based on electromagnetic induction 1015
J.H. Yang, K. Ye, G. Zhu & H. Guo

Influence of inductance on an interleaved parallel boost PFC circuit 1021
Z.H. Kong, L.G. Wu & Z.F. Luo

Author index 1025

VOLUME 2

Environmental science and environmental engineering

Research on carbon option pricing based on the real option theory 1033
H. Qiu

Sustainable development capacity of resource-based cities in the Beijing–Tianjin–Hebei region of China: A comparative study 1039
B. Li

$PM_{2.5}$ open-source component spectrum analysis in the harbor area 1047
Y. Lin

Distribution of oil spill risk on offshore facilities in the Bohai area based on ETA 1051
Y.B. Li, J.X. Liu & W.H. Wu

Developing a low-carbon economy and constructing a low-carbon city—a Xuzhou perspective 1055
W.Y. Zhang, C.L. Zhou, F. Chen & J. Ma

Geophysical and geochemical characteristics and mineralization potential in the Taonatu area, Inner Mongolia 1061
Q. Liu & R.M. Peng

Effects of genistein supplementation on exhaustive exercise-induced oxidative damage in mice 1065
Q.L. Hu, H. Huang & X.L. Huang

Modeling technologies for evaluation system of Jilin Province environmental protection 1069
J.Y. Dong & W. Cheng

Analysis and evaluation of the influence factors of waste packaging recycling in a circular economy 1073
N. Jiang, K. Liu & J.J. Zhang

Construction and application of a water recycling system in crab–crayfish polyculture purification 1077
X.S. Hang, F. He & F.Q. Gan

Sustainable energy industry coupled with social license to operate 1083
W. Shen & R.F. Li

Lab-scale treatment of biologically pretreated landfill leachate by the electro-Fenton process in a continuous flow reactor 1089
S.P. Yuan, X. Qin, L. Zhang & M.N. Zhou

The water and sediment characteristics numerical simulation of dig-in basin in strong tidal estuary 1095
G.-J. Zhang, C.-T. Lu, X.-F. Luo & Y.-F. Han

A method for detecting soil conditions of trenchless projects 1101
D.B. Fu, C. Xia & Y.F. Guo

Comparison of thermal hydrolysis and wet air oxidation in sludge treatment in China 1107
L. Peng & L.L. Hu

Enhancement of aerobic granulation with real domestic wastewater by powdered activated carbon addition 1113
C.W. Wang, B. Li, S.Y. Gong & Y. Zhang

Optimal water strategy for the United States 1117
H.-Y. Zheng, J.-C. Lu & M. Hu

A test study on the improved filler from blast furnace slag 1121
X.Y. Liu, G.Y. Xu & D.W. Huang

Environmental impact assessment of shipping construction based on the FCE method 1129
C. Xu & D.M. Yu

Analysis and prediction of energy sustainability in the developed regions of China 1135
P. Wang, X.J. Wang, Z.L. Wang & Y.B. Ren

The interaction between outflow dynamics and removal of NH_4^+-N in a vertical flow constructed wetlands treating septage 1141
Y.Y. Tan, F.E. Tang, A. Saptoro & E.H. Khor

Water use efficiency of the Lancang-Mekong River basin region in "the Belt and Road Initiative" 1147
C.Y. Xie, J.C. Feng & K. Zhang

An accessibility study of elevator Braille signage system in Da Nang City, Vietnam 1153
C.Y. Hsia, C.M. Huang & L. Tseng

Investigation and analysis of thermal comfort and IAQ in naturally ventilated primary school classrooms 1159
F.S. Ma, C.H. Zhan, X.Y. Xu & Y. Tang

Improvement of the ensemble forecast of typhoon track in the Northwestern Pacific 1167
J.Y. Yuan, Y. Pan & Y.P. Chen

An investigation into the system of feasibility study for the revitalizing of idle public facilities through outsourcing of venue management 1171
J.-H. Shyng

Distribution characteristics of ammonia emission from the livestock farming industry in Hunan Province 1175
X. Rong, C.H. Dai, Y. Deng & P.F. Qin

Application of aerobic bioremediation to cleanup octachlorinated dibenzofuran polluted soils 1181
J.L. Lin, Y.T. Sheu, C.M. Kao, W.P. Sung & T.Y. Chen

Experimental study on water-soil interaction influence for environmental change of marine soft soil 1185
H.-M. Liu, D. Zhou, H. Wu, W.-C. Jiao & Y.-T. Wang

Energy use and CO_2 emissions in China's pulp and paper industry: Supply chain approach 1193
C. Chen, R.Z. Qiu & J.B. Gan

Research on the limit equilibrium circle theory of entry support 1201
Q.-X. Huang, Y.-P. He, Z.-Q. Shi & J. Chen

Evolution characteristics of rainfall erosivity area based on the frequency analysis method in Zhejiang Province 1207
J.J. Zhang, G. Li & F.C. Lu

Research on the Norbulingka garden art characteristics under the background of Han-Tibetan cultural blending 1211
C. Liu & M. Wang

Releasing flux and characteristic of nitrous oxide from wastewater land treatment systems 1215
X.X. Zhang, Y.H. Li, Y. Wang & H.Y. Weng

A study of development planning for conservation areas in Taiwan 1219
T.-M. Lee

The study on the control optimization and strategy of indoor visual comfortable environment system 1223
D. Wang, H.W. Yin, P. Dong & Y.F. Chen

A study of a low-carbon and intelligent city index system 1229
Y.-S. Shen & H.-L. Liu

Exploring the lean strategies to obtain the banking loan for energy service companies 1233
A.K.C. Mei, Y.W. Wu, A.Y.P. Wu & C.C. Liu

In-plane lateral load resistance of cast in-situ mortar panels 1237
R. Iskandar, S. Suhendi & C. Lesmana

A discussion on how people perceive co-housing that facilitates intergenerational communication 1241
S.-Y. Tsai & C.-H. Ou

A note on the ABAQUS Concrete Damaged Plasticity (CDP) model 1247
W.S. Li & J.Y. Wu

The cutting parameter model of energy consumption and its characteristics analysis 1253
S.H. Hu, S.L. Li & J. Xie

Tibetan question parsing integrated with phrase structure and event feature 1259
N. Ma, H.Z. Yu, F.C. Wan & X.Z. He

Study on energy planning and partner selection problems in strategic alliances management of new energy industry 1265
J.Z. Zhai & X.N. Zhao

A fractal study on the surface topography of shearing marks 1271
B.C. Wang, C. Jing & L.T. Li

Computer simulation & computer and electrical engineering

Investigation of denoising methods of infrared imagery 1277
M.-K. Yue & J.-H. Deng

Feature optimization approach to improve performance for big data 1283
H. Zhu

Influence research on file of software defective testing configuration 1287
Y.X. Yu & L.Y. Wang

Webpage automatic summary extraction based on term frequency 1293
Y.X. Yu & L.Y. Wang

Research and optimization of the layout of F company truck interior workshop based on GA 1299
W. Jiang, Y.H. Ma & Y.C. Pan

The study and implementation of VoIP voice terminal system based on android platform 1303
G.J. Zhou

Research on a malicious code behavior acquisition method based on the Bochs virtual machine 1309
H.Y. Liu & Y.J. Cui

Research on the network security equipment allocation problem based on Monte Carlo tree search and machine learning 1313
C. Chen, H.J. Wang, N.W. Si & Y.Y. Liu

Robust automatic speech recognition based on neural network in reverberant environments 1319
L. Bai, H.L. Li & Y.Y. He

Application of association rule mining in electricity commerce 1325
H. Yang & Y.C. Pu

Research on a non-guided link discovery technology to obtain an early warning of financial risk 1331
C.Y. Xue

Effect of different operating media on the PVT system 1335
W. Pang, Y.Z. Zhang, H. Yan, Y. Liu & Y.N. Cui

A practical method for improving the coherence degree between SAR images 1339
W. Yu, Z.Q. Chang, X.M. Liu, W. Wang & J. Zhu

Smart management and control of household appliances 1343
Q.Y. Lu, S.Z. Chen & T.R. Li

Research and application of online monitoring and positioning systems for partial discharge of high-voltage cables 1347
T. Li, X.L. Zhang, Z.H. Wang, P.Y. Zhang & Y. Zhang

The numerical analysis of rainfall erosivity irregularity in Zhejiang province 1351
F.C. Lu, G. Li & J.J. Zhang

Module design of container architecture 1355
R.T. Zhu

Design of a reflective pulse oximetry sensing system based on the semi-active RFID tag 1361
L.Y. Chen, Y. Wang & H.W. Liu

Research of the long-range greenhouse environment monitoring system based on the cloud technology 1367
H.-W. Zhang, P.-J. Niu, H.-T. Tian & W.-F. Xue

Negative emotion speech classification for a six-leg rescue robot 1373
X.L. Han

Nonlinear vibration of a commensurate fractional-order happiness system 1379
Z.J. Guo & W. Zhang

Simulation analysis of airdrop cargo extraction posture 1385
H. Wang, X.-H. Chen, Y.-H. Zhou & X. Li

Research on the comparison between the compressed UF-tree algorithm and the UF-Eclat algorithm based on uncertain data 1389
C.Q. Chen, X.J. Guo, J.H. Huang & W.Q. Liao

Research on the sync technology of the ARINC659 bus redundancy fault-tolerant system 1395
Y. Li, X. Li & G. An

Identity recognition approach based on the improved phase congruency of the gait energy image 1401
L.-Y. Jia, C. Liang & D.-C. Shi

Fractional-order generalized augmented Lü system and its application in image encryption 1407
H.-Y. Jia & Y.-J. Wu

Ground operation efficiency analysis of a large airport airfield based on computer simulation 1411
X. Li, X.Q. Chen & D.X. Wei

Matrix search algorithm of robust common quadratic Lyapunov function for uncertain switched systems 1417
X.Y. Zhang, P. Li & B. Shen

HFSS simulation of RCS based on MIMO system 1425
Y.Y. Han, L. Sun & C. Hu

Object rough localization of tongue images via clustering and gray projection 1429
W.X. Liu, Z.C. Zhang, Y.Y. Lin, D.Y. Shen & Z.Y. Li

Multi-sensor attitude algorithm design for a low-cost strap-down system based on the direction cosine matrix 1437
J. Du, J. Li, C.J. Hu & K.Q. Feng

A study on personalized information push service based on context awareness and spatio-temporal correlation 1445
X.C. Wang, L.Y. Yuan & G.L. Ge

Design of a new in-flight entertainment terminal 1453
H.R. Xu, H. Zhou & H. Yang

The countdown traffic light error detection method based on union color spaces and fuzzy PCA 1459
S.Q. Mo, R. Zhang & Y.X. Wen

Study of the optimization evaluation algorithm of improved genetic-BP neural network in the monitoring and diagnosis of shortwave transmitting system 1465
Y. Luo & J. Gao

Loyalty model in the networked environment based on catastrophe 1473
Q.G. Liu & C.G. Yang

Research on obstacle avoidance of a mobile robot based on visual information 1479
J. Jiang

Multifocus image fusion based on defocus map estimation and NSCT 1483
R.X. Shi, F.J. Meng, D.L. Shan, P.P. Zeng & Y.L. Wang

A new and effective image retrieval method based on representative regions 1489
D.L. Shan, F.J. Meng, R.X. Shi, Y.L. Wang & P.P. Zeng

Semantic similarity research on case retrieval based on ontology 1493
Y.L. Liu, H. Duan & L. Luo

Vibration energy acquisition and storage management system based on MSMA 1499
Q.X. Zhang, K. Lin & J.K. Yang

Architecture of the on-chip debug module for a multiprocessor system 1505
K.X. Zhang & J. Yu

Load balancing algorithm for computing cluster using improved cultural particle swarm optimization 1511
W.H. Huang, Z. Ma, X.F. Dai, Y. Gao & M.D. Xu

An analysis of open source operating systems based on complex networks theory 1517
D.H. Zhang, Z.X. Zhao, Y.Q. Zhou & Y. Guo

Design of fitness information recording and network monitoring system based on BDS/GPS and Arduino Yun 1521
C. Jiang, J.Y. Wu, Y.X. Tu & Y.Y. Hu

A knowledge integration method for innovation teams based on social tagging in an open environment 1527
X.M. Li & X.F. Zhang

A study on the classification of Yunnan folk songs based on ensemble learning 1533
D. Wang, Y. Zhang & D.-J. Lv

RFID-based elevator positioning algorithm by the virtual reference label 1539
S. Zhang & X.-S. Zhang

Design of the omnidirectional mobile robot control system based on dSPACE 1545
H.-H. Liu, C.-S. Ai, H.-H. Zhao & X. Sun

An adapted NSGA-II approach to the optimization design of oil circuits in a hydraulic manifold block 1551
G. Li, W.T. Niu, W.G. Gao & D.W. Zhang

Quantification of single-event transients due to charge collection using dual-well CMOS technology 1559
Z. Zhang, W. He, S. Luo, L.X. He, Q.Y. Wu & J.M. Cao

Research on missing value processing methods based on advanced community detection 1565
F.Q. Zhao, G.J. Yang & X. Xu

Research on the knowledge discovery system in intelligent manufacturing based on the big data 1571
J. Li, X.Y. Liu, S.M. Jiang, Z.Q. Wei, S. Wang & J.F. Zhang

Study on the positioning system in China's Advanced Broadcasting System-Satellite 1577
M. Yan, J.-Y. Yang & X.-G. Wang

Finite element simulation of compression on micropillars 1583
G. Tang & Y.L. Shen

A neighborhood search algorithm for the unrelated parallel machine scheduling problem 1589
Y. Zhan & Y.G. Zhong

A novel medical image enhancement algorithm based on ridgelet transform 1593
Y.F. Yang & Y.W. Yang

Significance of deep learning on big data analytics 1597
J.L. Mao & Z.J. Mao

Branch pipe routing method based on a 3D network and improved genetic algorithm 1601
Y.X. Niu, W.T. Niu & W.G. Gao

Author index 1607

Civil, Architecture and Environmental Engineering – Kao & Sung (Eds)
© 2017 Taylor & Francis Group, ISBN 978-1-138-02985-9

Preface

The 2016 International Conference on Civil, Architecture and Environmental Engineering (ICCAE 2016) was held on November 4-6, 2016 in Taipei, Taiwan, organized by China University of Technology and Taiwan Society of Construction Engineers, aimed to gather professors, researchers, scholars and industrial pioneers from all over the world. ICCAE 2016 is the premier forum for the presentation and exchange of experiences, new advances and research results in the field of theoretical and industrial experience. The conference contained contributions promoting the exchange of ideas and rational discourse between educators and researchers from all over the world.

ICCAE 2016 is expected to be one of the most comprehensive Conferences focused on civil, architecture and environmental engineering. The conference promotes international academic cooperation and communication, and exchanging research ideas.

We would like to thank the conference chairs, organization staff, and authors for their hard work. By gathering together so many leading experts from the civil, architecture and environmental engineering fields, we believe this conference has been a very enriching experience for all participants. We hope all have had a productive conference and enjoyable time in Taipei!

Conference Chair
Dr. Tao-Yun Han
Chairman of Taiwan Society of Construction Engineers

Civil, Architecture and Environmental Engineering – Kao & Sung (Eds)
© 2017 Taylor & Francis Group, ISBN 978-1-138-02985-9

Organizing committee

HONOR CHAIRS

Prof. Ming-Chin Ho, *Architecture & Building Research Institute, Taiwan (Director General)*
Prof. Cheer Germ Go, *National Chung Hsin University, Taiwan*
Prof. Tzen-Chin Lee, *National United University, Taiwan*
Prof. Chu-hui Chen, *China University of Technology, Taiwan*

CONFERENCE CHAIRS

Prof. Jimmy C.M. Kao, *National Sun Yat-Sen University, Taiwan*
Prof. Yun-Wu Wu, *China University of Technology, Taiwan*
Prof. Che-Way Chang, *Chung-Hua University, Taiwan*
Dr. Tao-Yun Han, *Taiwan Society of Construction Engineers*
Prof. Wen-Pei Sung, *National Chin-Yi University of Technology, Taiwan*

CHAIR OF INTERNATIONAL TECHNOLOGICAL COMMITTEES

Prof. Ming-Hsiang Shih, *National Chi Nan University, Taiwan*

INTERNATIONAL TECHNOLOGICAL COMMITTEES

Yoshinori Kitsutaka, *Tokyo Metropolitan University, Japan*
Nasrudin Bin Abd Rahim, *University of Malaya, Malaya*
Lei Li, *Hosei University, Tokyo, Japan*
Yan Wang, *The University of Nottingham, UK*
Darius Bacinskas, *Vilnius Gediminas Technical University, Lithuania*
Ye-Cai Guo, *Nanjing University of Information Science and Technology, China*
Wang Liying, *Institute of Water Conservancy and Hydroelectric Power, China*
Gang Shi, *Inha University, South Korea*
Chen Wang, *University of Malaya, Malaya*

LOCAL ORGANIZING COMMITTEES (TAIWAN)

Wen-der Yu, *Chung Hua University, Taiwan*
Chien-Te Hsieh, *Yuan Ze University, Taiwan*
Ta-Sen Lin, *Taiwan Architects Association, Taiwan*
Hsi-Chi Yang, *Chung Hua University, Taiwan*
Jwo-Hua Chen, *Chienkuo Technology University, Taiwan*
Der-Wen Chang, *Tamkang University, Taiwan*
Cheng Der Wang, *National United University, Taiwan*
Shun-Chin Wang, *Architecture and Building Research Institute, Taiwan*
Yaw-Yauan Tyan, *China University of Technology, Taiwan*
Kuo-Yu Liao, *Vanung University, Taiwan*

Shih-Tsang Chou, *China University of Technology, Taiwan*
Shyr-Shen Yu, *National Chung Hsing University, Taiwan*
Yean-Der Kuan, *National Chin-Yi University of Technology, Taiwan*
Yu-Lieh Wu, *National Chin-Yi University of Technology, Taiwan*
Shih-Heng Tung, *National University of Kaohsiung, Taiwan*
Hsueh-Chun Lin, *China Medical University, Taiwan*
Yao-Chiang Kan, *Yuan Ze University, Taiwan*
Yao-Ming Hong, *Ming Dao University, Taiwan*
P.S. Pa, *National Taipei University of Education, Taiwan*
Shao-Wen Su, *National Chin-Yi University of Technology, Taiwan*
Yi-Ying Chang, *National Chin-Yi University of Technology, Taiwan*
Jun-Hong Lin, *Nanhua University, Taiwan*
Lei Wei, *National Chin-Yi University of Technology, Taiwan*
Ting-Yu Chen, *National Chin-Yi University of Technology, Taiwan*

Civil, Architecture and Environmental Engineering – Kao & Sung (Eds)
© 2017 Taylor & Francis Group, ISBN 978-1-138-02985-9

Acknowledgements

GUIDANCE UNIT

Construction and Planning Agency, Ministry of the Interior, R.O.C.
Architecture and Building Research Institute, Ministry of the Interior, R.O.C.

SPONSORS

Taiwan Society of Construction Engineers

中國科技大學
CHINA UNIVERSITY OF TECHNOLOGY

KEO

UNIVERSITAS KRISTEN MARANATHA

Structural science and architecture engineering

Civil, Architecture and Environmental Engineering – Kao & Sung (Eds)
© 2017 Taylor & Francis Group, ISBN 978-1-138-02985-9

Modeling two-dimensional rubble mound breakwater using dolos at armor layer and geotube at the core layer

O.C. Pattipawaej & H.J. Dani
Civil Engineering Department, Universitas Kristen Maranatha, Bandung, Jawa Barat, Indonesia

ABSTRACT: Coastal protection structure is used to protect the coast against erosion that is usually determined by the availability of materials at or near the job site, the sea conditions, water depth, and the availability of equipment for the implementation of the work. The purpose of this study is to conduct experimental research in the laboratory to obtain the rubble-mound breakwater design optimum and tools before it is applied directly in the field to reduce the risk of failure of construction. This study is conducted for laboratory testing of a two-dimensional rubble-mound breakwaters model with dolos at armor layer and geotube at core layer using regular wave and three variations of slope in front of the structure facing seaward, that is, 1:1.5, 1:2, and 1:2.5. The water level varies for the conditions of non-over-topping, over-topping, and submerged. The two-dimensional rubble-mound breakwaters model with the slope in front of the structure facing seaward 1:2.5 shows the most stable rubble-mound breakwater model.

1 INTRODUCTION

Indonesia as an archipelago country does not escape the impact of global warming due to the sea level rise. The impact of sea level rise results in the coastline change due to erosion and/or abrasion. In addition to global warming, forces of nature such as waves, currents, tides, and construction errors caused major damage to the existing breakwater. In general, construction fault lies in the tilt angle of the building, a thick layer, and heavy rock, in addition to other factors. This can lead to the collapse of the breakwater.

Breakwater is a structure on the coast to protect the coast against erosion. The type of breakwater structure used is generally determined by the availability of materials in or near the work site, the sea conditions, water depth, and the availability of equipment for the implementation of the work. Rubble-mound breakwaters use structural voids to dissipate the wave energy. Rock or concrete armor units on the outside of the structure absorb most of the energy, while gravels or sands prevent the wave energy's continuing through the breakwater core.

Construction of a breakwater on the field will take considerable time and cost. A laboratory test using a physical model is proved to be effective in avoiding such costs before constructing breakwater in the field. In this study, we will discuss the optimization of two-dimensional model of the rubble-mound breakwater using dolos at the armor layer and geotube at the core layer, because it has a high permeability that balances the water pressure. Wave run-up will be included in determining the peak elevation breakwater.

2 COASTAL PROTECTION STRUCTURE

Coastal structures are intended to protect shoreline or navigation channels from the effects of waves and other hydrodynamic force (Fith, et al., 2014). Design of coastal structures must consider a range of wave heights and periods combined with water level variations. The most common types of coastal structures are breakwaters. Breakwater is a structure constructed on coasts as part of coastal protection from the effects of both weather and longshore drift. Breakwater reduces the intensity of wave action in inshore waters and thereby reduces coastal erosion. Breakwaters may also be small structures designed to protect a gently sloping beach and placed at a distance of 1–300 feet offshore in relatively shallow water. Breakwaters can be constructed with one end linked to the shore, in which case they are usually classified as sea walls; otherwise, they are positioned offshore from as little as 100 m up to 300–600 m from the original shoreline. The types of breakwaters are rubble-mound structures, impermeable sloping structures, vertical wall structures, composite

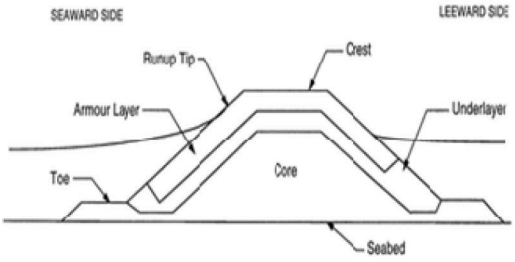

Figure 1. Cross section of a typical rubble-mound breakwater.

structures, floating structures, and pneumatic and hydraulic breakwaters (Hughes, 1993).

Rubble-mound structure is used extensively for breakwaters, jetties, revetments, seawalls, and wave absorber. Rubble-mound structures have a core of quarry-run stones, sand, slag, or other suitable materials protected from waves action by one or more stone under layers and a core layers of relatively large, selected quarry stones or specially shaped concrete armor units (Hudson, 1959). Rubble-mound breakwaters use structural voids to dissipate the wave energy. Rock or concrete armor units on the outside of the structure absorb most of the energy, while gravels or sands prevent the wave energy's continuing through the breakwater core. The integrity of a rubble-mound structure is primarily a function of the stability of the individual armor units that form the seaward face of the structure. In shallow water, revetment breakwaters are usually relatively inexpensive. As water depth increases, the material requirements and, hence, costs increase significantly. Figure 1 shows a typical cross section of a rubble-mound breakwater.

3 STABILITY OF RUBBLE-MOUND BREAKWATER

An important aspect in the design of a rubble mound is its stability to wave attack. Three aspects of the effect of waves on rubble-mound breakwater are wave run-up, overtopping, and transmission (Figure 2). Run-up is defined as the vertical height above still water level to which waves incident upon a structure can be expected to travel up the face of the structure. Wave run-up is important in defining both the amount of wave energy transmitted over and through permeable rubble-mounds and also the quantity of water that may be expected to overtop the structure (Hur, Lee, and Cho, 2012).

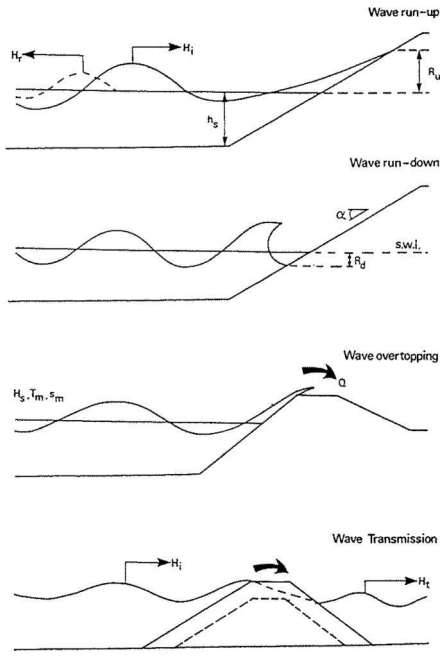

Figure 2. Waves on rubble-mound breakwater.

4 EXPERIMENT SETUP AND PROCEDURE

The experimental test was conducted on the wave flume at Laboratory Balai Pantai, Ministry of Public Works in Buleleng, Bali, Indonesia. The wave flume is 40 m long, 0.6 m wide and 1.2 m high. It is equipped with a piston-type wave generator that produces regular wave. Figure 3 shows three wave probes that are installed in the wave flume.

Simulation of the wave generated by the wave maker uses regular wave model. The model of rubble-mound breakwater is constructed with the seaward face at slopes 1:1.5, 1:2, and 1:2.5 using an armor layer composed of individual units of weight W and density ρ. The armor units use dolos with the average weight of 265 g, relative density of 2.209 g/cm^3, and K_d of 8. The dolos is randomly placed at the armor layer (CIRIA, 2007). The core layer is set to be stable by using geotube. Three variations of slopes facing the seaward side of the breakwater model are applied: 1:1.5, 1:2, and 1:2.5. The wave period is 2 s. The wave height for different slopes of breakwater models can be seen in Table 1.

The water level tests are conducted at four different water levels: 38 cm (mean low water level), 54 cm (mean high water level), 63 cm (crest elevation), and 70 cm (submerged). The structure is assumed to be founded on an impermeable bed, and the duration of exposure to waves is not considered.

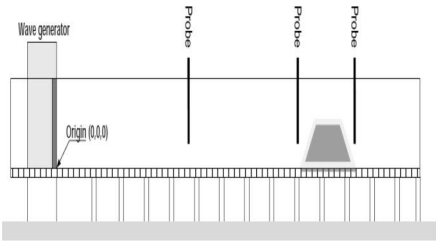

Figure 3. Side view of the flume.

Table 1. Wave heights at different slope of breakwater model.

Slope	Wave height (cm)
1:1.5	12.42
1:2	13.66
1:2.5	14.72

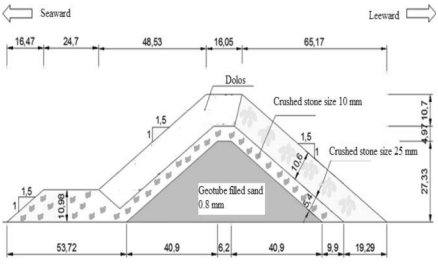

Figure 4. Side view of rubble-mound breakwater model with slope of 1:1.5.

The rubble-mound breakwater model is designed on the basis of the stability of rubble-mound structure using the Hudson formula (Hudson, 1959). The similarity of the rubble-mound breakwater model is 1:10. Figure 4 presents the side view of the rubble-mound breakwater model with the slope of 1:1.5.

5 RESULT AND DISCUSSION

Wave direction, either normally incident or oblique, refers to the direction of wave travel with respect to the breakwater axis. Tables 2–4 present the results of wave height measured using zero upcrossing statistic in front of rubble-mound structure model with slopes 1:1.5, 1:2, and 1:2,5 facing the seaward side, respectively. The highest wave height occurred at crest elevation.

The significant wave height, runup, and rundown at 38 cm of water elevation can be seen in Table 5. It can be concluded that $H_{1/3}$ and $Ru - R_d$ at the mean low water level show the lowest values at the slope 1:2.5 of the rubble-mound breakwater model. It means that the highest energy of wave absorption occurred at the slope of 1:2.5 facing the seaward side of the rubble-mound breakwater model.

When the water level is 54 cm or at the mean high water level, only rundown occurred. The rundown for each different slope of the rubble-mound breakwater model is shown in Table 6. The wave absorber gives the highest value for the slope of 1:2.5 for the rubble-mound breakwater model.

The elevation of the crest should be minimum at which overtopping occurs. This should be based on maximum wave runup (Palmer and Christian,

Table 2. Wave heights based on zero upcrossing statistics in front of rubble-mound structure with slope 1:1.5 facing the seaward side.

Water level (cm)	H_{max} (cm)	$H_{1/3}$ (cm)	$H_{1/10}$ (cm)	$H_{average}$ (cm)
70	18.0	15.5	16.7	14.4
63	27.0	25.8	26.3	23.9
54	16.2	15.4	15.9	14.1
38	15.5	13.7	14.5	11.5

Table 3. Wave heights based on zero upcrossing statistics in front of rubble-mound structure with slope 1:2 facing the seaward side.

Water level (cm)	H_{max} (cm)	$H_{1/3}$ (cm)	$H_{1/10}$ (cm)	$H_{average}$ (cm)
70	18.5	16.2	16.7	13.4
63	19.9	18.5	19.1	16.7
54	14.3	14.0	14.1	13.1
38	15.9	14.5	15.0	13.0

Table 4. Wave heights based on zero upcrossing statistics in front of rubble-mound structure with slope 1:2.5 facing the seaward side.

Water level (cm)	H_{max} (cm)	$H_{1/3}$ (cm)	$H_{1/10}$ (cm)	$H_{average}$ (cm)
70	17.9	15.7	16.3	14.9
63	18.1	17.3	17.7	16.0
54	17.6	16.7	17.1	15.4
38	13.8	12.6	13.1	11.3

Table 5. Significant wave height, runup, and rundown at 38 cm of water elevation.

Format of slope	$H_{1/3}$ (cm)	Runup, R_u (cm)	Rundown, R_d (cm)	$R_u - R_d$ (cm)
1:1.5	13.7	32.0	8.5	23.5
1:2	14.5	28.0	8.0	20.0
1:2.5	12.6	20.0	6.0	14.0

Table 6. Rundown at the mean high water level.

Format of slope	Rundown, R_d (cm)
1:1.5	14.5
1:2	17.0
1:2.5	22.0

Table 7. Wave transmission coefficient at the water level 70 cm.

Slope	H_t(cm)	H_i (cm)	K_t
1:1.5	13.1	15.5	0.85
1:2.0	9.0	16.2	0.56
1:2.5	8.3	15.7	0.53

1998). Unfortunately, the overtopping at 63 cm of water elevation cannot be recorded due to the instrument's problem during the experiment.

The wave transmission coefficient (K_t) is defined as the ratio of the transmitted wave height (H_t) at the leeside to the incident wave height (H_i) at the breakwater seaward, as follows:

$$K_t = \frac{H_t}{H_i} \quad (1)$$

The value of K_t indicates the effectiveness of a rubble-mound breakwater at submerged condition to attenuate waves (Yuliastuti and Hashim, 2011, Zhang and Li, 2014). The value of K_t varies between 0 and 1. A value of zero implies that there is no transmission, whereas 1 means no reduction in wave height (there is no barrier in front of the wave). The result of wave transmission coefficient is presented in Table 7 at the water level of 70 cm (submerged).

On the basis of the result of wave transmission coefficient, slope 1:2.5 of the rubble-mound breakwater model can reduce the wave height more significantly than the slopes 1:1.5 and 1:2 of the breakwater model.

6 CONCLUSIONS

The function of rubble-mound breakwater is to protect the coastal area. Because the rubble-mound breakwater needs to be stable, the two-dimensional physical model of rubble-mound breakwater is conducted using three different slopes, 1:1.5, 1:2, and 1:2.5, facing the seaward side. The water levels are applied at the mean low water level, the mean high water level, the crest elevation, and submerged using the flume with regular wave. The rubble-mound breakwater model is designed on the basis of stability of this breakwater using the Hudson formula. The armor units of the rubble-mound breakwater model are dolos placed randomly facing the seaward side. The core is set stable using geotube. The wave absorber, transmission wave, and displacement of armor units give the best result for the slope of 1:2.5 of the rubble-mound structure model.

The results of two-dimensional physical testing for this rubble-mound breakwater model will certainly be helpful in making the optimum slope of rubble-mound breakwater facing the seaward side in coastal areas of Indonesia with erosion and/or abrasion condition. The results of the two-dimensional rubble-mound breakwater model will be very useful if it can proceed to the next stage of the three-dimensional physical test by using regular and irregular waves. In addition, test results of physical model of this structure can also improve the existing rubble-mound breakwater, especially damaged rubble-mound breakwater.

ACKNOWLEDGMENTS

The authors thank DIPA Kopertis Wilayah IV, Ministry of Research, Technology, and Higher Education, the Republic of Indonesia, for providing the grant accordance with the Letter Agreement of Implementation Research Grant No. DIPA-023.04.1.673453/2015, on November 14, 2014, and the first revision on March 3, 2015. They also thank Balai Pantai, Ministry of Public Works, for providing the research facilities to undertake the research.

REFERENCES

CIRIA, CUR, CETMEF. 2007. *The Rock Manual*. The use of rock in hydraulic engineering, 2nd edition, C683, CIRIA, London.

Fith, L.B., et al. 2014. Between a rock and hard place: Environmental and engineering considerations when designing coastal defense structure. *Coastal Engineering*. 87:122–133.

Hudson, R.Y. 1959. Laboratory Investigation of Rubble mound Breakwaters. *Journal of the Waterways and Harbors Division, American Society of Civil Engineers* 85(WW3): 93–121.

Hughes, S.A. 1993. Physical Models and Laboratory Techniques in Coastal Engineering. *Advanced Series on Ocean Engineering* 7. River Edge, NJ: World Scientific Publishing Co. Pte. Ltd.

Hur, D.S., Lee, W.D. and Cho, W.C. 2012. Characteristics of wave run-up height on a sandy beach behind dual-submerged breakwaters. *Ocean Engineering* 45: 38–55.

Palmer, G., and Christian, C.D. 1998. Design and construction of rubble mound breakwaters. *IPENZ Transactions*, 25(1).

Yuliastuti, D.I. and Hashim, A.M. 2011. Wave transmission on submerged rubble mound breakwater using L-blocks. *2nd International Conference on Environmental Science and Technology IPCBEE* 6, Singapore: IACSIT Press.

Zhang, S.X. and Li, X. 2014. Design formulas of transmission coefficients for permeable breakwaters. *Water Science and Engineering* 7(4): 457–463.

Civil, Architecture and Environmental Engineering – Kao & Sung (Eds)
© 2017 Taylor & Francis Group, ISBN 978-1-138-02985-9

Shear stress calculation of rubber asphalt overlay and stress-absorbing layer

Jizong Tan
Guangxi Key Laboratory of Road Structure and Materials, Nanning, China
Guangxi Transportation Research Institute, Nanning, China

Jianguo Wei
Guangxi Key Laboratory of Road Structure and Materials, Nanning, China
Changsha University of Science and Technology, China

Chan Pan
Guangxi Key Laboratory of Road Structure and Materials, Nanning, China
Guangxi Transportation Research Institute, Nanning, China

Kaixi Huang
Guangxi Communications Professional Technology Institute, Nanning, China

ABSTRACT: By using BISAR mechanical calculation software to calculate and analyze the rubber asphalt compound pavement shear stress of different interlayer adhesive states and under the condition of stress-absorbing layer thickness, we know that the adhesive states of stress-absorbing layer, rubber asphalt surface layer, and underlying cement pavement have a direct impact on the distribution of shear stress of asphalt overlay and stress-absorbing layer, and the maximum shear stress of asphalt layer bottom will first decrease and then increase with the increase of friction parameters. Therefore, the bottom layer should have good adhesion to prevent the premature entry of shear stress growth period.

1 PREFACE

The stress-absorbing layer is arranged on the general cement concrete deck and asphalt surface layer, which can effectively disperse the stress concentration of cement concrete joints or cracks under load effect in order to delay or prevent the appearance of reflective crack of asphalt pavement. The commonly used stress-absorbing layer types mainly include the layer distribution method stress absorbing layer (such as SAMI), modified asphalt mixture stress absorbing layer, the compound stress absorbing interlayer, geosynthetics, and synchronous macadam transition layer, among which the first three have better impermeable, crack resisting, and bonding properties, whereas the effect of the latter two in the practical application is not significant. The cost of modified asphalt stress absorbing layer and compound stress absorption interlayer engineering is high, and the difficulty of construction is relatively high. By contrast, the layer distribution method stress absorbing layer is relatively more economical, reasonable, and convenient for construction. Rubber powder-modified asphalt with high elasticity, toughness, and high deformation is more applicable to the layer distribution method stress absorbing layer. In addition, the rubber powder-modified asphalt stress absorbing layer is also an effective measure of waste tires.

The layer distribution method for rubber powder-modified asphalt stress absorption layer is widely used in compound pavement engineering; however, some technical problems still remain to be solved, including setting rubber powder-modified asphalt binder stress-absorbing layer asphalt overlay design theory and method of structure, the rubber asphalt binding material to improve the technical performance, and the construction technology and other aspects. In light of this, the above rubber asphalt stress-absorbing layer shear characteristics are studied in this paper, in order to further improve the technology of rubber powder-modified stress absorbing layers.

2 ANALYSIS OF THE INTERLAMELLAR SHEAR STRESS

The combination form of general rubber asphalt compound pavement structure is shown in Fig. 1.

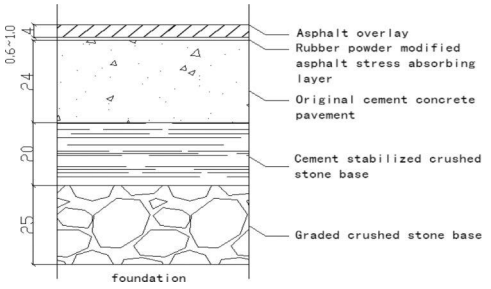

Figure 1. Pavement structure combination.

Table 1. Pavement structure parameters.

Structure layer	Thickness (cm)	Modulus (MPa)	Poisson's ratio
Asphalt overlay	4.0	1200	0.35
Absorbing layer	0.6~1.0	400	0.35
Cement concrete	24.0	30000	0.15
Cement-stabilized stone base	20.0	1500	0.20
Graded stone	25.0	350	0.35
Soil matrix	–	100	0.40

In addition to the rubber powder-modified asphalt stress-absorbing layer structure of each layer of compressive resilient modulus and Poisson's ratio, we refer to "asphalt pavement design specification" -JTG D50-2006 value. However, the rubber powder-modified asphalt stress-absorbing layer refers to the modified asphalt stress-absorbing layer parameters. The values of the pavement material parameters for each layer are shown in Table 1.

Using BISAR pavement structure in Table 1 in the interlayer under BZZ-100 standard axle load conditions, shear stress is calculated to analyze the thickness of the shear stress distribution, contact conditions, the interlayer shear stress, and the effects of stress-absorbing layer thickness on shear stress.

2.1 *Distribution of shear stress in the lower layers of different adhesive states*

In this analysis, the stress-absorbing layer and the upper and lower positions under different conditions of friction parameters ∂ each point along the driving direction (0,1a,2a,3a) at the XX and YY normal stress component analysis asphalt surface and the bottom of the maximum stress absorbing layer shear stress distribution. The results are shown in Figures 2–6.

As can be seen from Figures 2–6, the maximum shear stress distribution of the stress-absorbing compound pavement overlay and the stress absorbing underlying layer can be changed with different adhesive statuses, and the main changes are as follows:

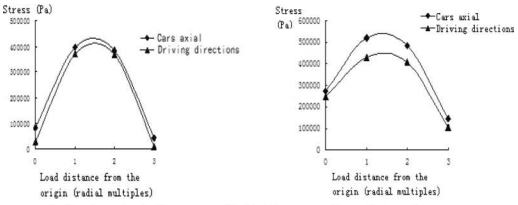

（a）Asphalt layer （b）Stress-absorbing layer

Figure 2. Shear stress at the underlying layer under the condition of complete continuity between two layers.

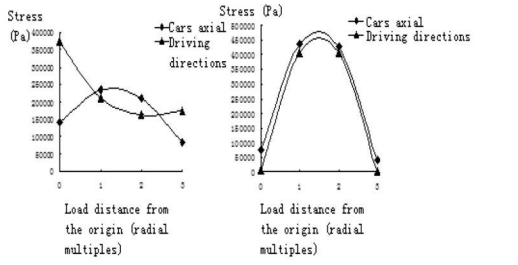

（a）Asphalt layer （b）Stress-absorbing layer

Figure 3. Shear stress at the underlying layer when the upper layer is 0.5.

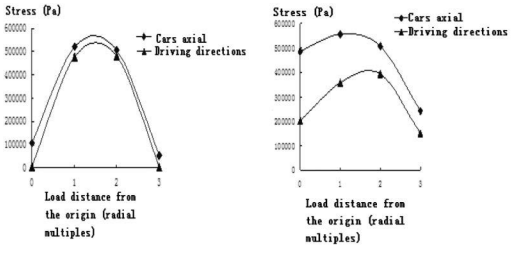

（a）Asphalt layer （b）Stress-absorbing layer

Figure 4. Shear stress at the underlying layer when the upper layer is completely sliding.

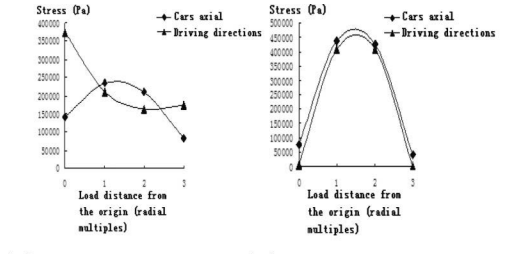

（a）Asphalt layer （b）Stress-absorbing layer

Figure 5. Stress absorbing layer friction parameter is 0.5.

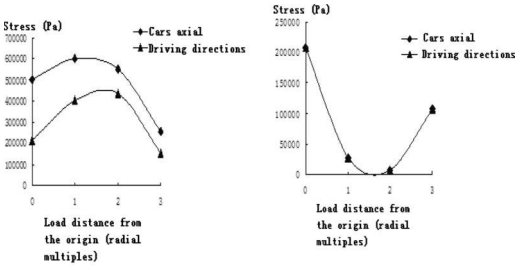

（a）Asphalt layer （b）Stress-absorbing layer

Figure 6. Shear stress at the underlying layer when the absorbing layer is completely sliding.

Table 2. Shear compliance under different friction parameters.

Adhesive layers	Friction parameters	Modulus (MPa)	Poisson's ratio	AK (N/m^2)
Asphalt overlay and stress-absorbing layer	0	1200	0.35	0
	0.25			3.99E-11
	0.5			1.20E-10
	0.75			3.59E-10
	0.99			1.19E-08
Stress-absorbing layer with the original concrete pavement	0	400	0.35	0
	0.25			1.20E-10
	0.5			3.59E-10
	0.75			1.08E-09
	0.99			3.56E-08

1. When every level of compound pavement is completely in continuous state, asphalt layer and stress-absorbing layer stress was basically consistent along the direction of travel distribution, and auto axial and driving direction stress are all parabolas, and the axial stress is always greater than the direction of traffic stress.
2. When an adhesive status between the asphalt surface layer and the stress-absorbing layer changes, the distribution of stress in asphalt overlay takes a significant change along the directions of traffic. When the friction parameter is in the case of 0.5, the axial stress and stress variation of the direction of travel are exactly opposite, and the maximum shear stress is travel direction stress in load center, which proves that the interlayer adhesive status affects the stress distribution of the asphalt surface layer and the maximum shear stress direction. At the same time, under three friction parameter conditions, absorbing layer stress changing rules along the direction of traffic are not obvious, but there still exists possibility of the presence of the influence of different friction parameters on stress variation.
3. When the stress-absorbing layer and the original cement coagulation pavement adhesive status change, the variation of asphalt overlay and stress-absorbing layer of stress were significantly changed. When the friction parameter is 0.5, that is to say, when the stress-absorbing layer and the cement concrete road surface are not fully bonded, the stress distribution is basically equal to the effect generated the asphalt layer—the changing adhesive status of the stress-absorbing layer. Changes in stress distribution stress-absorbing layer occurs when incomplete bonding is not large; however, when the layers completely coincide, the driving direction and the distribution of the axial stress are exactly opposite with fully bonded case, namely the maximum shear stress is seen as a parabola, which decreases first and then increases.
4. From the distribution of stress in different layers and the variation of bonded conditions, it can be seen that the interlayer shear stress distribution varies, and this effect will change with the variation of friction parameters.

2.2 *Variation of maximum shear stress between the layers with different bond states*

BISAR is used to make mechanical analysis for stress-absorbing layer and the upper and lower positions, respectively, under different conditions of friction parameters. The friction parameters were 0, 0.25, 0.5, 0.75, and 0.99, in which the friction parameter 0 is for complete adhesion and 0.99 is for nearly complete slide. The variation of the maximum shear stress under different conditions of friction parameters is shown in Figs. 7 and 8.

As shown in Figures 7 and 8, the change of the bonding condition between stress absorption layer and the upper and lower layers affects the maximum shear stress between itself and the bottom layers of asphalt directly. With the increase in friction parameters between asphalt layer and stress-absorbing layer, the maximum shear stress

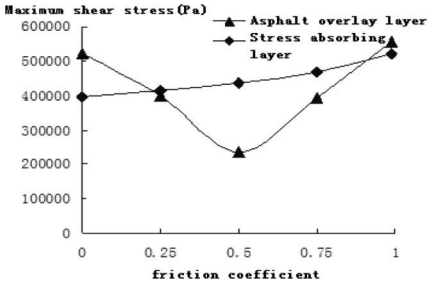

Figure 7. Maximum shear stress at the bottom of the layer under the condition of friction parameter of different asphalt overlay stress-absorbing layer.

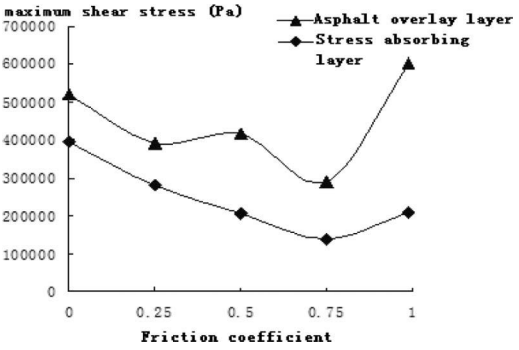

Figure 8. Maximum underlying shear stress between cement pavement and stress-absorbing layer under the condition of different friction parameter.

of rubber asphalt overlay will first decrease and then increase with the increase of friction parameters, while the maximum shear stress of the bottom stress absorption layer increases with it. The good bonding state of asphalt overlay layer can reduce the maximum shear stress of the stress absorption layer and prevent the premature failure of the stress absorbing layer. Although the change trend of asphalt overlay was first reduced and then increased, reducing the maximum shear stress of asphalt overlay by reducing the bonding degree between layers is not suitable, because at the beginning of building, the initial bonding state between the layers is not ideal. At the same time, over time, the bonding condition of interlayer will be gradually reduced, so it should not be the measures to prevent premature to enter the maximum shear stress growth. The bonding condition between the stress-absorbing layer and the cement pavement has a significant impact on the maximum shear. The maximum shear stress of rubber asphalt overlay and stress absorption layer bottom will first decrease and then increase with the increase of friction parameters. And for the asphalt layer bottom, completely sliding and in relatively complete bonding condition, the maximum shear stress increases by 15.23%, which also proves that we cannot reduce the maximum shear stress by reducing the adhesion of the layers.

2.3 *Effect of different stress-absorbing layer thicknesses on the maximum shear stress of the bottom layer*

BISAR is used for the mechanical analysis of rubber asphalt overlay (stress-absorbing layer) under different conditions of stress-absorbing layer thickness.

The thicknesses were 0, 0.6, 0.7, 0.8, 0.9, 1.0 and 1.5 cm. It can be found from calculation that when we do not set stress-absorbing layer, the maximum shear stress of the asphalt overlay bottom layers is 5.959 × 105, and the calculation results of bottom shear stress when settings with other different thickness of stress absorption layer are as shown in Figure 9.

As it can be seen from Figure 9, with the increase in the thickness of stress-absorption layer, the maximum shear stress between asphalt overlay and the bottom stress-absorbing layers decreases continuously, the maximum shear stress decreases by 12.59% when stress absorbing layer thickness is set at 0.6 cm. When the thickness is 1.0 cm, it decreases by 23.55%, and when the thickness is 1.5 cm, under the maximum shear stress, it decreases by 32.01%, which proves that the thickness effect is the effective measure to reduce the maximum shear stress of asphalt pavement; however, this effect increases with the thickness gradually. At the same time, for rubber powder-modified asphalt stress-absorbing layer, its thickness is 0.6–1.0 cm, and in the actual use of the process, because of the influence of Webster effect, the lower layer of asphalt will form a certain thickness of the oil-rich layer, the actual reduction effect of the maximum shear stress is greater than the one of calculation results. Therefore, the rubber powder-modified asphalt stress-absorbing layer is an economical and reasonable anticracking measure. In addition, from the variation of the maximum shear stress of absorption bottom layer in different thickness, it can be seen that increasing thickness cannot effectively reduce the maximum shear stress of stress-absorption layer. When the thickness of the stress-absorbing layer increases from 0.6 to 1.0 cm, the maximum shear stress decreases by only 3.44%. When the thickness of the stress-absorbing layer increases to 1.5 cm, the maximum shear stress decreases by only 7.5%. Therefore, the increasing of thickness of the stress-absorbing layer cannot effectively reduce the maximum shear stress by itself, which requires the stress-absorbing layer material's good elastic recovery, and the rubber powder asphalt has

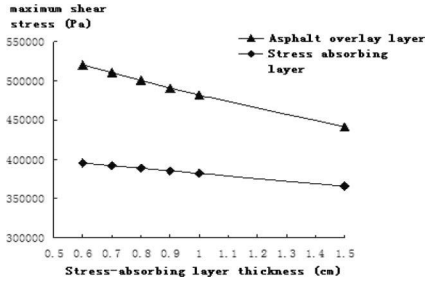

Figure 9. Bottom layer maximum shear stress under different thicknesses of stress-absorbing layer.

a high modulus and a high viscoelasticity trait, which is in line with this request.

3 CONCLUSION

1. By using BISAR mechanical calculation software, we calculated and analyzed the rubber asphalt compound pavement shear stress of different interlayer adhesive states, and under the condition of stress-absorbing layer thickness, we knew that the adhesive states of stress-absorbing layer, rubber asphalt surface layer, and underlying cement pavement have a direct impact on the distribution of shear stress of asphalt overlay and stress-absorbing layer, and the maximum shear stress of asphalt layer bottom will first decrease and then increase with the increase in friction parameters. Therefore, the bottom layer should have good adhesion to prevent the premature entry of shear stress growth period.
2. With the increase in the thickness of the stress-absorbing layer, the maximum shear stress of asphalt overlay is significantly reduced, but the effect of the maximum shear stress of the stress-absorbing layer is not obvious.

ACKNOWLEDGMENT

Guangxi Key Lab of Road Structure and Materials 2013 Open Subject, 2013gxjgclkf-004.

REFERENCES

Department of Transportation Highway Science Research Institute. Thin Layer Asphalt Concrete Surface Layer Technology Research [R]. Beijing: 2004.

Guan Chang Yu, Wang Zheren, Guo Dazhi. Study on the Bonding State of Pavement Structure Layer [J]. Chinese Journal of Highway, 1989, 2(1): 70–80.

Huang Xiaoming, Liao Gongyun. Application of ABAQUS Finite element software in road engineering [M]. Nanjing: Southeast University press, 2008.

Ruymbeke E. van, Keunings R., V. Stephenne. Determination of the Molecular Weight Distribution of Entangled Linear Polymers from Linear Viscoelasticity Data. Journal Non Newtonian Fluid Mwch. 2002.

The Ministry of transport of the people's communist country. Specifications for design of highway asphalt pavement (JTG D50–2006). Beijing; People's Communication Press, 2006.

Thomas Bennert, Ali Masher, and Joseph Smith. Evaluation of Crumb Rubber in Hot Mix Asphalt. Final Report[R]. Department of Civil and Environmental Ehgineering, Rutgers University. 2004.